

Open Research Online

The Open University's repository of research publications and other research outputs

Explosive volcanism in complex impact craters on Mercury and the Moon: influence of tectonic regime on depth of magmatic intrusion

Journal Item

How to cite:

Thomas, Rebecca J.; Rothery, David A.; Conway, Susan J. and Anand, Mahesh (2015). Explosive volcanism in complex impact craters on Mercury and the Moon: influence of tectonic regime on depth of magmatic intrusion. *Earth and Planetary Science Letters*, 431 pp. 164–172.

For guidance on citations see [FAQs](#).

© 2015 Published by Elsevier B.V.



<https://creativecommons.org/licenses/by-nc-nd/4.0/>

Version: Accepted Manuscript

Link(s) to article on publisher's website:

<http://dx.doi.org/doi:10.1016/j.epsl.2015.09.029>

Copyright and Moral Rights for the articles on this site are retained by the individual authors and/or other copyright owners. For more information on Open Research Online's data [policy](#) on reuse of materials please consult the policies page.

oro.open.ac.uk

Explosive volcanism in complex impact craters on Mercury and the Moon: influence of tectonic regime on depth of magmatic intrusion

Rebecca J. Thomas ^a, David A. Rothery ^a, Susan J. Conway ^a and Mahesh Anand ^{a,b}

^a Department of Physical Sciences, The Open University, Walton Hall, Milton Keynes, MK7 6AA, UK

^b Department of Earth Sciences, Natural History Museum, Cromwell Road, London, SW7 5BD, UK

Corresponding author: Rebecca J. Thomas, Department of Physical Sciences, The Open University, Walton Hall, Milton Keynes, MK7 6AA, UK, rebecca.thomas@open.ac.uk, +44 (0)1908 858535.

Abstract

Vents and deposits attributed to explosive volcanism occur within numerous impact craters on both the Moon and Mercury. Given the similarities between the two bodies it is probable that similar processes control this spatial association on both. However, the precise morphology and localization of the activity differs on the two bodies, indicating that the nature of structures beneath impact craters and/or volcanic activity may also be different. To explore this, we analyze sites of explosive volcanism within complex impact craters on the Moon and Mercury, comparing the scale and localization of volcanic activity and evidence for post-formation modification of the host crater. We show that the scale of vents and deposits is consistently greater on Mercury than on the Moon, indicating greater eruption energy, powered by a higher concentration of volatiles. Additionally, while the floors of lunar craters hosting explosive volcanism are commonly fractured, those on Mercury are not. The most probable explanation for these differences is that the state of regional compression acting on Mercury's crust through most of the planet's history results in deeper magma storage beneath craters on Mercury than on the Moon. The probable role of the regional stress regime in dictating the depth of intrusion on Mercury suggests that it may also play a role in the depth of sub-crater intrusion on the Moon and on other planetary bodies. Examples on the Moon (and also on Mars) commonly occur at locations where flexural extension may facilitate shallower intrusion than would be driven by the buoyancy of the magma alone.

Keywords

Mercury

Moon

explosive volcanism

impact crater

intrusion

1. Introduction

It has long been recognized that vents and deposits attributed to explosive volcanism frequently occur within complex impact craters on the Moon [e.g., Schultz, 1976; Head and Wilson, 1979; Coombs and Hawke, 1992]. More recently, data from the MErcury Surface, Space ENvironment, GEochemistry, and Ranging (MESSENGER) spacecraft have revealed that an association between putative explosive volcanism and impact craters also exists on Mercury [Gillis-Davis et al., 2009; Thomas et al., 2014b]. Mercury and the Moon are similar in several respects: they are virtually airless, and have a surface geology that is dominated by a combination of impact cratering and volcanic resurfacing. The similar localization of explosive volcanic activity on both bodies, therefore, suggests the action of similar processes.

In the lunar case, it has been proposed that localization of explosive volcanism within impact craters results from density-trapping of magma in the brecciated zone below the crater [Head and Wilson, 1979]. In this model, a vertically-propagating dike encounters the low density, weak material of the breccia lens beneath the crater floor and is diverted to form a sill because the density and rigidity contrast favors lateral propagation rather than continued vertical ascent [Schultz, 1976; Wichman and Schultz, 1995a]. With continued recharge, this sill propagates horizontally until it encounters higher lithostatic pressures at the wall zone [Thorey and Michaut, 2014] and the intrusion begins to thicken, fracturing the floor above. Dike propagation to the surface is commonly favored along zones of extension at the intrusion margins [Pollard and Johnson, 1973] and results in either effusive volcanism, forming lava pools, or, if sufficient exsolved gas builds up prior to eruption, explosive volcanism [Jozwiak et al., 2015]. The products of both of these styles of volcanism are observed at

54 circumferential fractures in floor-fractured craters (FFCs) on the Moon, so this appears to be a good
55 explanatory model.

56 On Mercury, too, there is evidence for sub-crater magma storage prior to eruption. Endogenic pits
57 surrounded by a spectrally-distinct deposit, interpreted as volcanic vents [Kerber et al., 2009], often
58 occur in groups within a single crater, indicating a shared proximal source for coeval and/or
59 sequential eruptions. Moreover, the scale and morphology of vents and deposits are consistent with
60 accumulation of volatiles in a subsurface magma chamber prior to eruption [Thomas et al., 2014b].
61 The occurrence of the majority (79%) of explosive volcanic vents surrounded by putative pyroclastic
62 deposits within impact craters on Mercury also supports the hypothesis that the subsurface structure of
63 craters plays a controlling role in the localization of explosive volcanism. However, the specific
64 character of this volcanism differs from that on the Moon. Floor-fracturing is observed in only one
65 impact crater on Mercury [Head et al., 2009], and this does not host a pyroclastic vent or deposit.
66 Additionally, explosive volcanism commonly occurs at and around central uplifts in craters on
67 Mercury, rather than at the outer margin of the floor [Thomas et al., 2015].

68 The contrasting character of volcanism and host-crater modification between the Moon and Mercury
69 indicates that it cannot be assumed that magma rise beneath impact craters on terrestrial bodies will
70 always result in the eruptive character familiar from the Moon. An investigation into probable
71 controls on crater-localized magma rise, storage, and explosive eruption on each body has the
72 potential to enhance our understanding of tectono-magmatic conditions on both bodies. To this end,
73 we have investigated the dimensions and settings of pits and deposits thought to result from explosive
74 volcanism within complex impact craters on the Moon and Mercury. Using these data, we have
75 characterized the energy of eruption and deformation of host craters and thereby placed constraints on
76 the probable controls on intrusion and eruption. Our findings suggest that the regional stress regime
77 played an important role in the depth of magma intrusion on Mercury, and may also have done so on
78 the Moon.

2. Data and methods

2.1 Site selection

We analyzed 16 sites on Mercury and 15 on the Moon where an impact crater hosts candidate volcanic vents surrounded by a diffuse-margined spectral anomaly generally accepted to indicate a pyroclastic deposit (Table S1). Only sites occurring within complex impact craters were selected (30-120 km diameter on Mercury [Pike, 1988] and 30-140 km on the Moon [Pike, 1980]), so that subsurface crater-related structures could be considered broadly comparable across the sample set.

On both bodies, examples were drawn from previously identified sites where putative pyroclastic deposits appear to have been sourced from candidate vents within the crater structure, and where those vents are evident in topographic data. On this basis, and choosing examples only where the presence of a pyroclastic deposit is relatively uncontroversial, 15 lunar examples were drawn from 41 possible sites [Wolfe and El-Baz, 1976; Head and Wilson, 1979; Coombs and Hawke, 1992; Gaddis et al., 2003; Gustafson et al., 2012]. A sample of 16 sites was drawn from 71 identified sites on Mercury [Kerber et al., 2011; Thomas et al., 2014b]. These selection criteria, choosing examples that are least-controversial and most amenable to analysis on each body, may mean that the samples do not reveal the full range of variation in pyroclastic activity within complex craters on either body.

2.2 Pyroclastic deposits

Identification of putative pyroclastic deposits on both Mercury and the Moon relies primarily, at present, on observation of a diffuse-margined spectral anomaly in orbital images. Deposits believed to be pyroclastic on Mercury have higher reflectance and a steeper (“redder”) slope of spectral reflectance versus wavelength than the planetary average. To identify them, we constructed composites combining reflectance data from the 996 nm, 749 nm and 433 nm filters in MESSENGER’s 10.5° field-of-view Wide Angle Camera (WAC) in the red, green, and blue channels, respectively, in which they appear as a bright, orange spectral anomaly (Figure 1a). We constructed composites from all images created prior to October 17th, 2013 having a resolution of 1000 m/pixel or better, and also examined the PDS-hosted 1000 m/pixel global color mosaic (March 2014 release).

Lunar pyroclastic deposits are commonly identified by their low albedo relative to highlands material and a spectral character suggesting varying mixtures of highlands, basaltic and glass components [Gaddis et al., 2003]. We identified the extent of putative deposits on the basis of a low-albedo, diffuse-margined anomaly in the 1489 nm apparent reflectance mosaic from the Moon Mineralogy Mapper (M3) on the Chandrayaan-1 spacecraft, and in a color composite combining 1000 nm, 900 nm and 415 nm global mosaic reflectivity data from the Clementine spacecraft in the red, green and blue bands (Figure 1b).

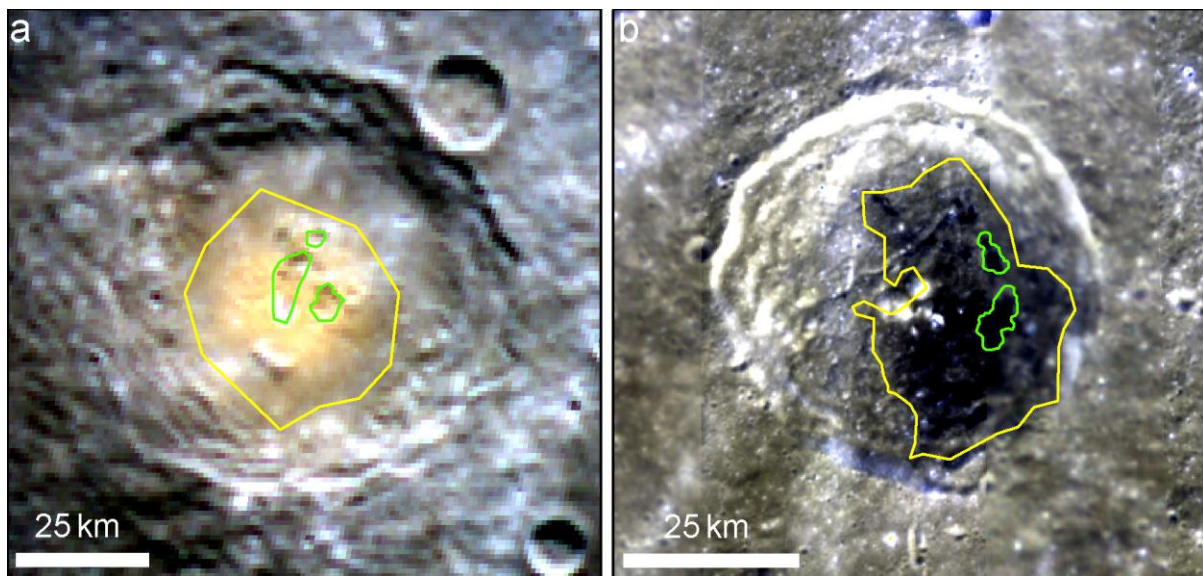


Figure 1. Spectral anomalies with diffuse margins interpreted as pyroclastic deposits on (a) Mercury and (b) The Moon. Yellow outline: extent of the spectral anomaly, green outline: rim of candidate vent. (a) Rilke crater (pit group 8026). Color composite of MDIS WAC images EW0222970395I (996 nm), EW0222970415G (749 nm), and EW0222970399F (433 nm) (NASA/JPL-Caltech) in the red, green and blue bands. (b) Franklin crater. Excerpt from the Clementine UVVIS global mosaic with reflectance at 1000 nm, 900 nm, and 415 nm and in the red, green and blue bands.

For both bodies, we digitized the areal extent of the spectral anomaly, taking a conservative approach by excluding the tenuous outer fringe. This was further refined in lunar examples where the extent of the low albedo material is apparent as fine-grained material mantling the underlying terrain in high-resolution narrow-angle camera (NAC) images from the Lunar Reconnaissance Orbiter Camera (LROC). As a means of calculating the maximum specific energy with which particles were ejected

from vents, we additionally measured the maximum distance between a candidate vent (Section 2.3) and the outer margin of its surrounding continuous deposit at each site. Because the available data types and the spectral character of deposits differ on the two bodies, the same level of error cannot be assumed in determination of the position of the outer boundary of the deposit. We estimated it as 2 pixels, but it may be higher, particularly on Mercury where there are no high-resolution images with which the position of this outer boundary can be refined. This introduces a bias in favor of larger detected deposits on the Moon. Comparisons of deposit areal extent on the two bodies are therefore made with caution.

2.3 Volcanic vents

On Mercury, irregular, rimless depressions lacking the characteristic ejecta blanket of impact craters (known as ‘pits’) are considered candidate volcanic vents [Kerber et al., 2011]. These are readily identifiable in monochrome orbital imagery taken by the NAC and WAC in MESSENGER’s Mercury Dual Imaging System (MDIS) (Figure 2a-b). We obtained topographic data with which to determine the volume of these vents by using stereo images (NAC or WAC frames using the 750 nm filter) to create high-resolution DEMs by photogrammetry using the Ames Stereo Pipeline [Moratto et al., 2010]. Point data were averaged on a 3x3 block of pixels, giving the DEM a horizontal resolution 3 times larger than that of the stereo images used to create it. On the basis of error determinations made by Thomas et al. [2014b], the vertical error is up to 80 m.

We identified candidate lunar vents by reference to the LROC WAC Global mosaic at 100 m/pixel, higher-resolution NAC images, and the Lunar Orbiter Laser Altimeter 188 m/pixel DEM. Identification of vents within putative explosive volcanic deposits is less certain on the Moon than on Mercury because lunar examples commonly occur within floor-fractured craters. Relatively wide sub-circular regions of the crater-floor grabens, particularly where these occur within an intense part of the albedo anomaly, are interpreted as the probable source of the surrounding pyroclastic deposit (Figure 2c-d).

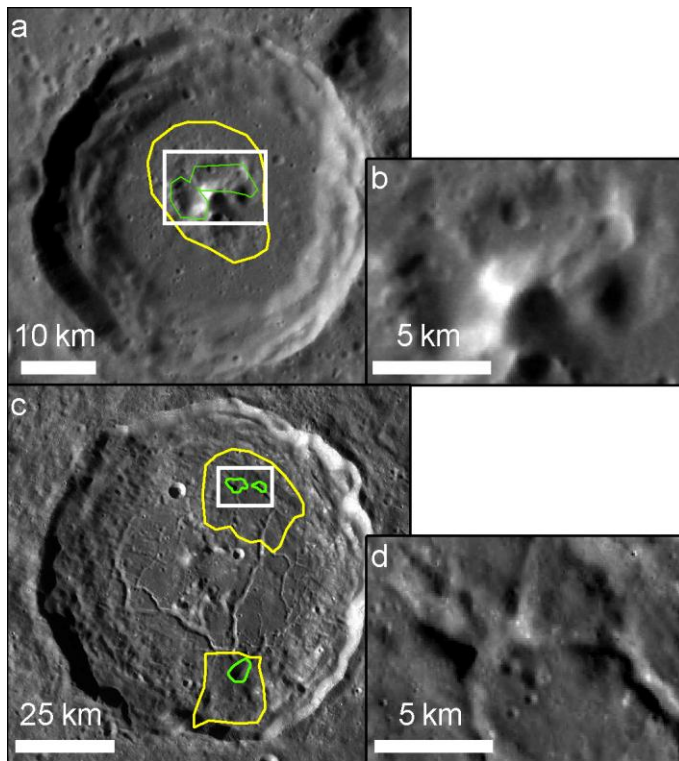


Figure 2. Characteristic appearance of crater-hosted candidate explosive volcanic vents on (a,b) Mercury and (c,d) the Moon. Green outline = vent rim, yellow outline = extent of surrounding spectral anomaly. Close-ups (b) and (d) indicated by white rectangles. (a-b) Pit group ID 6083 (MDIS NAC image EN0251000097M; NASA/JPL-Caltech). (c-d) Atlas crater (excerpt from the LRO WAC Global mosaic).

Volcanic vents commonly form by erosion of wall-rock during eruption and/or by collapse into an evacuated magma chamber. Therefore the volume of the vent can indicate the energy or volume of eruption. In order to calculate the volume of material that was lost to form the identified vents, we calculated their volume below a rim elevation determined with reference to orbital imagery and topographic products. On both bodies, though to a greater degree in floor-fractured craters on the Moon, the original surface prior to vent-formation was uneven. To account for this when calculating the volume lost to form the vent, we used a Natural Neighbor technique within ArcGIS software to interpolate a surface at the vent rim level on the basis of the surrounding topography, and subtracted elevations on the vent floor from the elevation of that surface. Because this interpolation technique estimates elevation values on a local basis, any relief owing to a pre-existing graben crossing the vent is greatest at the margins of the interpolated area and reduces towards the interior. This means that the

original graben volume is only partially accounted for, and the calculated volume of vents within grabens should be viewed as a maximum value.

2.4 Host crater dimensions

The intrusion of magma beneath impact craters on the Moon is proposed to result in a reduction in crater depth [Schultz, 1976]. To explore this, we calculated the host crater depth for all sites in the two samples, defined as the vertical distance between the average rim crest elevation and the average floor elevation. In finding the average rim elevation, we excluded parts of the rim crest where major post-formation modification was evident. The average crater floor elevation was defined as the 100 m bin within which the highest number of DEM pixels in the interior of the crater fell. We compared the depth thus calculated to the depth calculated using depth-diameter relationships observed in large populations of mature complex craters [Pike, 1980, 1988]. For craters on the Moon where floor-fracturing is observed, we used two methods to calculate the minimum effective thickness (T_e) of overburden consistent with the observed uplift if this had been the result of sub-crater intrusion, using material constants as listed in Thorey and Michaut [2014] and Jozwiak et al. [2015], respectively. The method developed by Thorey and Michaut [2014] uses the finding that uplift will have a convex morphology if the flexural wavelength of the overburden is less than a quarter of the crater floor radius. If this uplift extends laterally to the wall zone, the crater floor radius can thus be used to calculate the minimum elastic thickness of the overburden. This method is appropriate for ten craters in our sample. Conversely, Pollard and Johnson [1973] calculate the effective thickness of the overburden based on the magmatic driving pressure required to uplift overlying material to the observed uplift radius. Though this approach has been criticized [Thorey and Michaut, 2014], we include the results of this method as a basis for comparison with other studies [e.g., Wichman and Schultz, 1995a, 1995b; Jozwiak et al., 2012, 2015]. We noted any extensional or compressional tectonic structures within the crater, making reference to global datasets [Jozwiak et al., 2012; Byrne et al., 2014], and any evidence (such as burial of the central uplift) for post-crater-formation lava infilling.

2.5 Regional setting

To assess possible regional controls on the occurrence of explosive volcanism, we studied the geological setting of each site in detail. This included noting the proximity to and spatial relationship with extensive lava plains, association with specific substrates and types of tectonic structure, and proximity to other sites of explosive volcanism. For Mercury, we made reference to the global MESSENGER monochrome and color mosaics, individual MDIS images, and published maps of smooth plains [Denevi et al., 2013] and tectonic structures [Byrne et al., 2014]. For the Moon, we referred to published geological maps and the global LROC WAC mosaic.

3. Results

3.1 Vent and deposit scale

The average volume of an individual vent at sites on the Moon ($0.54 \pm 0.06 \text{ km}^3$) is significantly smaller than on Mercury ($25.0 \pm 2.1 \text{ km}^3$) (Figure 3a), despite the potential for overestimation of vent volume on the Moon (Section 2.3). The range in volume across the sample set is also lower: $0.002 \pm 0.007 - 6.75 \pm 1.96 \text{ km}^3$ on the Moon and $0.08 \pm 0.08 - 454 \pm 58.6 \text{ km}^3$ on Mercury. To investigate whether these differences are because of a more distributed style of volcanism on the Moon than on Mercury, we compared the total vent volume at each site on the two bodies and found that this, too, is significantly smaller on the Moon (average $1.9 \pm 0.34 \text{ km}^3$) than on Mercury (average $47.0 \pm 3.9 \text{ km}^3$) (Figure 3b).

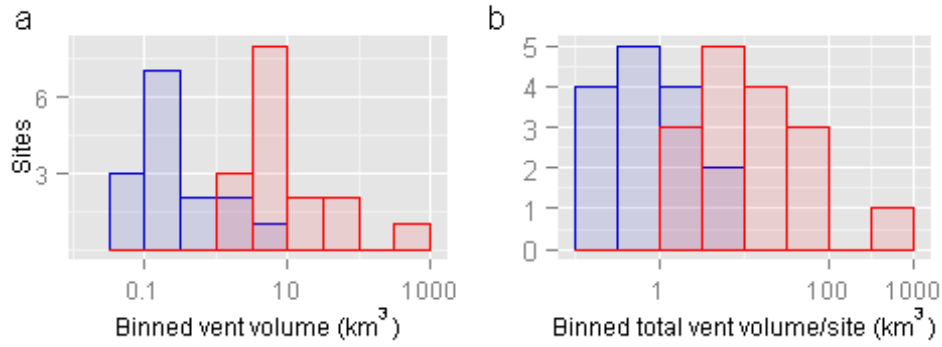


Figure 3. Vent volumes on the Moon (blue) and Mercury (red). Both (a) the average volume and (b) total volume of vents at a site are significantly lower on the Moon than on Mercury (note the logarithmic scale for the x-axes).

The maximum ballistic range measured for particles forming the observed deposit is generally higher on Mercury (median value of 18.6 ± 1.2 km, maximum of 50.3 ± 1.2 km) than on the Moon (median 10.7 ± 0.04 km, maximum 46.6 ± 0.04 km) despite the observational bias in favor of detection of pyroclastic material to greater distances on the Moon and despite higher gravity on Mercury, which means that particles ejected at equal velocity will have a smaller range than on the Moon. Because lunar vents commonly occur as a relatively subtle widening of a graben, it is probable that in some cases particle sources have been missed and the ballistic range overestimated. We therefore also compare the average geodetic area of deposits within our sample sets. This, too is larger for Mercury (median 1210 ± 53.2 km², maximum 6990 ± 138 km²) than for the Moon (median 231 ± 5 km², maximum 3949 ± 22 km²), supporting the inference that particles were, on average, ejected to greater distances on Mercury. The maximum ballistic range (X) can be used to calculate the maximum speed (v) at which pyroclasts were ejected from a vent in a vacuum using the relationship:

$$X = \frac{v^2}{g} \sin 2\theta ,$$

where g is gravitational acceleration and θ is the angle at which dispersal is greatest (45°). This gives a value of 284 m s^{-1} for the median and 468 m s^{-1} for the greatest ballistic range observed in the Mercury sample set, and 143 m s^{-1} for the median and 297 m s^{-1} for the greatest ballistic range

observed in the lunar sample set. As the specific energy of particle ejection is approximately proportional to the volatile mass fraction in the released magma [Wilson, 1980], this indicates a higher concentration of volatiles in the eruptions on Mercury than on the Moon, for volatile species of similar molar mass. This is consistent with findings for the entire global populations [Kerber et al., 2011; Thomas et al., 2014b].

3.2 Tectonic modification of host craters

14 of the sites on the Moon lie within impact craters catalogued as floor-fractured [Schultz, 1976; Jozwiak et al., 2012], and cover a range of documented FFC types (Table S1). The anomalously shallow, fragmented floor of the crater Hell, which hosts the remaining site, suggests that this may also be an FFC. This high correlation to FFCs is also observed in the global population of putative pyroclastic deposits hosted by complex craters: 12 of the non-sampled 26 host craters are previously-catalogued FFCs, and 9 are flooded by mare lavas that would obscure any floor-fracturing, if present. One (Grimaldi F) is crossed by a graben of regional extent and vents in another (Messala) are aligned along grabens in the crater floor. Of the remaining three sites, we suspect that the ‘pyroclastic deposits’ at Lagrange C and Schluter A are spectrally-distinct impact ejecta, and, though Vitruvius has not previously been catalogued as a floor-fractured crater, its morphology is consistent with that of an FFC modified by volcanic deposition. Thus, it appears that floor-fracturing of craters hosting localized pyroclastic deposits on the Moon is almost ubiquitous. Candidate vents occur in concentric fractures adjacent to the crater wall at 10 of the sampled sites and adjacent to the crater central uplift at only two. The crater floor depth ranges from 38% to 83% of the expected depth of a crater of that diameter. Because the shallow depth of these craters does not appear to result from mare-infilling, and because of the fractures present on the crater floors, uplift by a sub-crater intrusion is the most probable explanation of their shallow rim-to-floor depths.

The calculated minimum effective thickness (T_e) of crust overlying intrusions capable of producing the observed uplift ranges from 0.9 to 5.3 km for convex-floored craters using the method of Thorey and Michaut [2014], and 0.6 to 4.0 km over the whole sample set using the method of Pollard and Johnson [1973] (Figure 4). Where there is a piston-like uplift and the crater is not large (e.g., Haldane,

Kopff), intrusions are expected to be significantly shallower [Thorey and Michaut, 2014]. Because T_e is the thickness of a single layer with the observed flexural rigidity, and crater floor materials are heterogeneous and may contain some weaker layers, the true thickness of the overburden is expected to be considerably greater than T_e . If, after Wichman and Schultz [1995a], we approximate it as $6 \times T_e$ for lunar FFCs, and if we approximate the transient crater depth as one third of the transient crater diameter (D_{tr}) [Grieve and Cintala, 1982] and calculate D_{tr} as $D_t^{0.15} D^{0.85}$ after Croft [1985] where D_t (the transition diameter between simple and complex impact craters on the Moon) is 17.5 km [Pike, 1980] and D is the observed rim–rim diameter, in all cases the approximated intrusion depth is equal to or less than that of the transient crater below the crater floor. This may indicate that intrusion occurred along the base of the fallback breccia zone but, given the uncertainty of the estimated values used in these calculations, this cannot be considered proven.

Extensional crater floor fractures are not observed at the sites on Mercury. Minor thrust faults cross two of the host craters. Otherwise, apart from central uplifts and relief proximal to candidate vents, the floors are flat, and there is no evidence of flexure over a larger region beyond the crater floor. Crater depths vary from 57% to 120% of the value predicted by the depth-diameter ratio for fresh craters observed by Pike [1988], and fall well within the range of depth-diameter ratios for complex craters observed by Baker and Head [2013] (Figure 5). Anomalously shallow craters have larger diameters, as has been observed for non-fresh impact craters on Mercury in general and attributed in large part to post-formational modification by infilling [Barnouin et al., 2012]. A smooth, shallow flat floor with only a small central peak projecting above it at six of the sampled sites indicates that this is a probable modification mechanism. Thus, our findings support post-formational shallowing of host craters, but there is no evidence that this occurred by tectonic uplift. At fourteen of the sixteen sites, vents occur at the crater center.

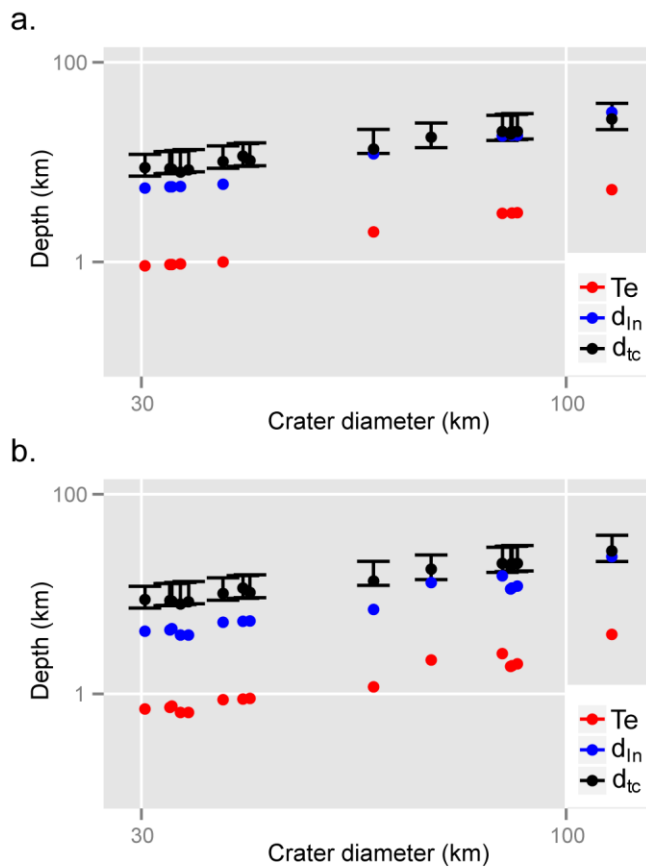


Figure 4. Effective thickness (T_e) of overburden consistent with (a) crater floor radius where there is convex uplift (Thorey and Michaut [2014] method) and (b) uplift radius (Pollard and Johnson [1973] method) within sampled lunar FFCs compared with the estimated depth of the transient crater below the present-day crater floor (d_{tc}). d_{in} is $6 \times T_e$, an estimate of intrusion depth.

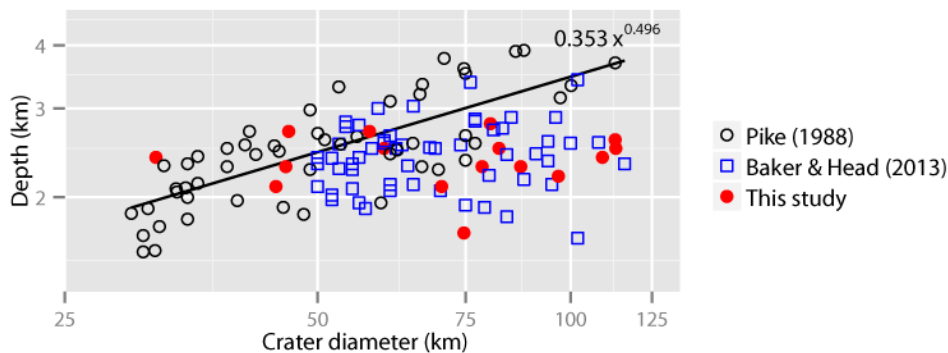


Figure 5 Depth versus diameter of craters on Mercury, comparing those in this study with larger populations of complex craters measured by other authors. Black line indicates the d-D relationship observed by Pike [1988] for mature complex craters.

3.3 Association with regional geological units and tectonic structures

Craters hosting pyroclastic deposits in the lunar sample set commonly superpose, are adjacent to, or are in areas annular to extensive basin-filling mare deposits. The distance to the edge of a major mare deposit ranges up to 340 km, with a mean distance of 90 km. Conversely, sites on Mercury are not commonly adjacent to morphologically young large-scale lava plains, which range from 90 to 1540 km distant, 800 km on average (Figure 6).

The sampled sites on Mercury are often in regions hosting many other sites of putative explosive volcanism. Seven sites overlie the relatively low-reflectance LRM substrate. This relationship is particularly apparent in an elevated, extensively thrust-faulted region centered on 136.8° E, 45.4° S, where four of the sampled craters lie within 350 km of each other, along with many other centers of putative pyroclastic volcanism (Figure 7). In this region, the lowest-reflectance surface material comprises the walls and proximal ejecta of large (> 80 km diameter) relatively fresh craters. The depth to which such craters excavate can be estimated as > 15 km [Croft, 1985], indicating that this substrate is present to considerable depth. At three of the sampled sites the crater also hosts hollows, which are rimless depressions thought to form by loss of a relatively volatile substance from the planet's surface [Blewett et al., 2013; Thomas et al., 2014a].

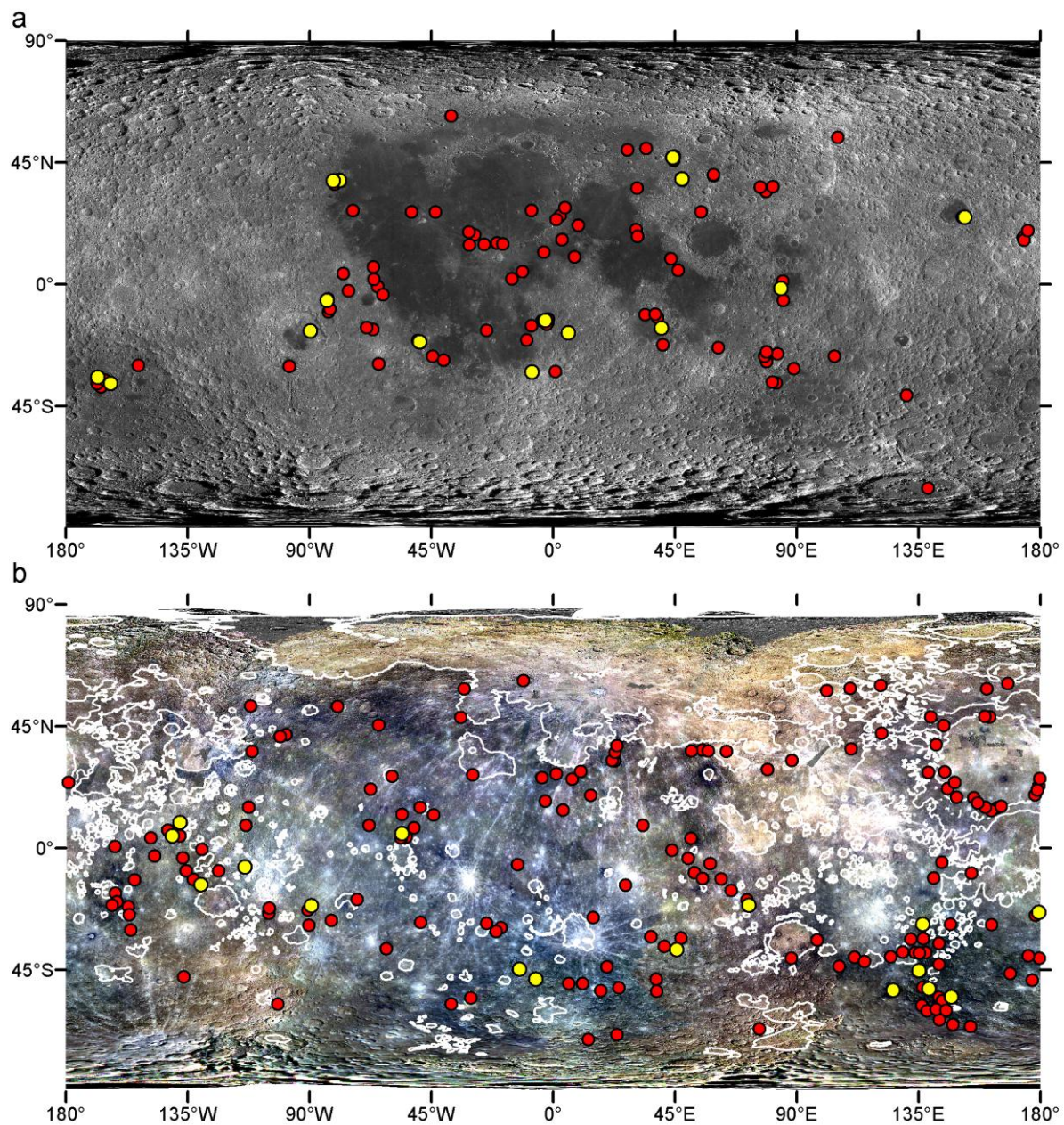


Figure 6. Sampled (yellow circles) and all (red circles) sites with putative pyroclastic activity on (a) the Moon and (b) Mercury (white outline: extent of smooth volcanic plains [Denevi et al., 2013]). Base images: LRO WAC global mosaic and MDIS global color mosaic.

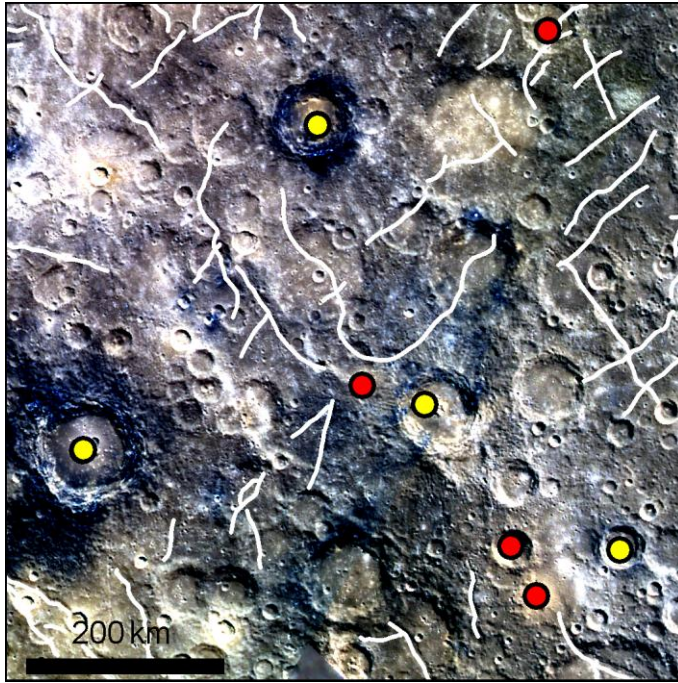


Figure 7. A cluster of sites of explosive volcanism on LRM substrate on Mercury. Dots: yellow = sampled sites, red = not in sample set. White lines: contractional landforms [Byrne et al., 2014] (mosaic of color composites combining MDIS WAC images EW1012828676I, EW1012828668G and EW1012828664F, and EW0230923343I, EW0230923363G and EW0230923347F; NASA/JPL-Caltech).

4. Discussion

4.1 Scale and energy of eruption

Consistent with findings for the global population [Kerber et al., 2011; Thomas et al., 2014b], the maximum velocity at which pyroclasts were ejected at our sampled sites of explosive volcanism on Mercury is greater than at those on the Moon. Additionally, vents are larger on Mercury, though the higher gravity dictates that dikes should be narrower and mass fluxes lower [Wilson and Parfitt, 1989] than on the Moon. If the vents formed primarily through erosion of wall-rock during eruption, larger vents indicate higher eruption energy, consistent with the high ejection velocity. This in turn supports the inference, made on the basis of global dataset, of an on average higher volatile mass fraction in the released magma in explosive volcanism on Mercury than on the Moon [Kerber et al., 2011; Thomas et al., 2014b].

Volcanic vents can also form through collapse or subsidence into a magma chamber, and have been proposed to do so on Mercury [Gillis-Davis et al., 2009]. If this process contributed to vent-formation on both planets, the larger vent size on Mercury indicates higher volume eruption. Unfortunately, the low resolution of the topographic data on Mercury at present precludes calculation of the erupted volume; so, the importance of this process cannot be investigated. A further method by which a large vent can form is by sequential eruption at closely-spaced loci, forming a compound vent. There is evidence that this does occur on Mercury [Rothery et al., 2014]. If eruption were more localized at sites on Mercury, this process would lead to larger vents. However, as the summed vent volume at each site is significantly higher on Mercury than the Moon, overlapping vents on Mercury cannot be the prime explanation for the contrast in vent volume.

4.2 Implications for sub-crater magma storage on Mercury

The high incidence of floor-fracturing in complex craters hosting pyroclastic deposits on the Moon and its absence at such sites on Mercury requires explanation. Floor-fracturing on the Moon is proposed to occur due to sub-crater magmatic intrusion. An alternative hypothesis, that it occurs due to viscous relaxation [Hall et al., 1981], has been found to be inconsistent with the geometry and spatial variability of most FFCs [Wichman and Schultz, 1995a; Jozwiak et al., 2012]. Therefore, the absence of floor-fracturing within complex impact craters on Mercury may simply indicate that dikes propagate directly to the surface without a period of near-surface magma storage. At sites where a small-scale pyroclastic deposit surrounds a single vent, we cannot preclude this possibility. However, there are multiple vents at five of the sampled sites, and at another there are two large vents close by in an overlapped crater (Figure 8). This suggests the presence of a magma reservoir in the shallow subsurface from which multiple eruptions were sourced, either in a coeval or a sequential manner. Additionally, unless Mercury's mantle is exceptionally enriched in volatiles, the high eruption velocities necessary to form the more extensive spectral anomalies by pyroclastic volcanism strongly suggest a period of storage prior to eruption, during which volatiles became concentrated through magmatic fractionation [Thomas et al., 2014b]. We note that the maximum ballistic range indicated by the extent of putative pyroclastic deposits is not significantly larger at sites where the presence of

multiple vents provides supporting evidence for pre-eruption crustal storage than at other sites. This may indicate that, as on the Moon, sub-crater storage occurs prior to eruption in all or most cases.

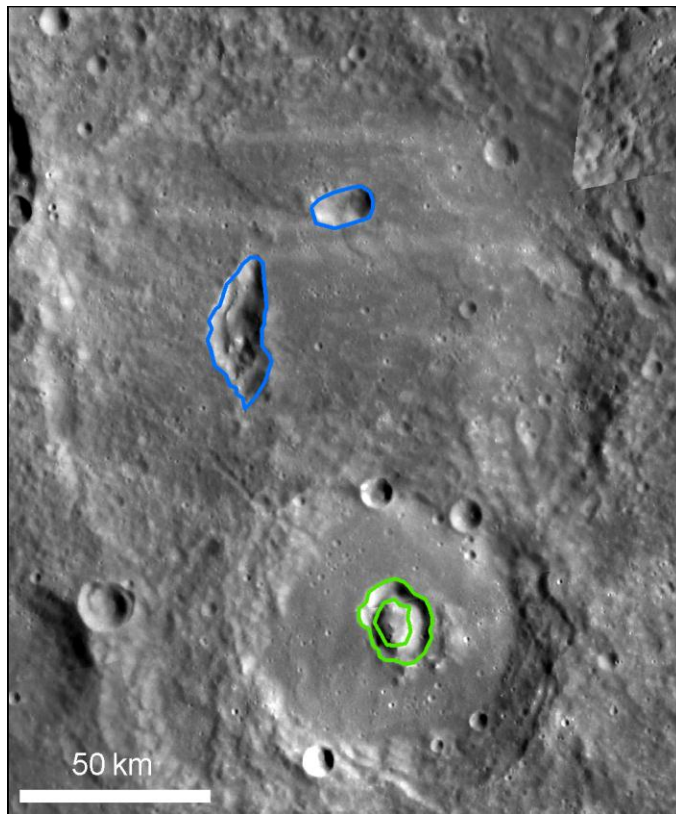


Figure 8. Two intersecting craters hosting vents surrounded by putative pyroclastic deposits (-72.2° E, -19.6° N). Pit outlines: green = vent at sampled site 5023, blue = vents not within the sample set. Base image: mosaic of MDIS NAC images EN0219177174M and EN0219092124M (NASA/JPL-Caltech).

One possible contributing factor to a lack of surface deformation in response to a subsurface intrusion on Mercury is that the overburden is stronger than on the Moon. This could result from more voluminous impact melt [Grieve and Cintala, 1997] or less porosity [Collins, 2014] due to higher impact velocity and gravity, or from infilling by massive lavas prior to the proposed explosive volcanic activity. Numerical and physical modeling is necessary to determine the degree to which these factors could affect the bulk strength of sub-crater-floor materials, though the differences would need to be large if they were to account for the total lack of surface deformation seen in host craters on Mercury.

The major factor governing surface deformation above a magma body is the depth of intrusion. Deeper intrusion on Mercury would be consistent with the common localization of vents at the crater's central uplift, which are expected to be bounded by multiple high-angle, deep-going faults [Scholz et al., 2002; Senft and Stewart, 2009; Kenkmann et al., 2014]. These are zones of weakness along which dike propagation from relatively deep reservoirs to the surface would be favored. On the basis of buoyancy alone, deeper intrusion on Mercury is not favored. All other factors being equal, the higher gravity on Mercury means that a smaller thickness of overburden produces a given lithostatic pressure, leading to a shallower level of neutral buoyancy (LNB). Moreover, density contrasts between magmas and the crust also favor deeper intrusion on the Moon. Magmas forming picritic glasses believed to have been erupted in lunar pyroclastic eruptions are calculated to be denser ($2850 - 3150 \text{ kg/m}^3$ [Wieczorek et al., 2001; Vander Kaaden et al., 2015]) than the highlands crust within which most of our sample occurs (Table S1) (bulk density 2550 kg/m^3 [Wieczorek et al., 2013]), rendering it necessary to invoke conditions such as excess pressure at the base of the crust [Head and Wilson, 1992] and superheating of the source magma [Wieczorek et al., 2001] to explain the surface eruption of these magmas in the highlands. Conversely, elemental abundance data show a continuity of compositions between smooth volcanic plains and the heavily-cratered regions within which our sampled sites on Mercury occur [Weider et al., 2015], supporting the inference from spectral data that these heavily-cratered surfaces may simply be ancient volcanic plains [Murchie et al., 2015]. This suggests that, contrary to deeper magma storage being favored, hot, volatile-bearing Hermean magmas are expected to be so buoyant that effusive eruption will occur without a period of sub-surface storage, except where the crust has anomalously low density. Thus in addition to the evidence presented here for deeper magma storage beneath impact craters on Mercury than on the Moon, the additional problem arises that the observed frequent occurrence of volcanic activity within impact craters [Thomas et al., 2014b], where ascent should be *least* favored (due to underlying low-density breccia), is the opposite of what is expected on the grounds of magma buoyancy.

However, the above applies only if an LNB is reached, whereas there is abundant evidence [e.g., Takada, 1989] that it is rarely reached in nature. The level of magma rise is commonly controlled by

the presence of rheological or rigidity contrasts in the overburden [Menand, 2011]; indeed the rigidity and density contrast at the base of the impact crater brecciated zone is proposed to account for the depth of sub-crater magma intrusion on the Moon. However, a deeper low-rigidity zone on Mercury does not appear to be supported. Modeling suggests that, due to higher average impact velocities, it will instead be shallower [Cintala, 1979; Barnouin et al., 2011]. Another important control on the depth of magma storage, and one that provides a good explanation for both volcanism within impact craters on Mercury and its depth relative to that on the Moon, is the regional stress field. This has been compressive on Mercury through much of the planet's history [Strom et al., 1975], while compressive tectonics are observed only at a small scale and in the recent past on the Moon [Watters et al., 2010]. On Earth, upper-crustal magma storage is deeper in compressive than in extensional regimes [Chaussard and Amelung, 2014]. Numerical simulations support this observation, showing that in a compressive regime, vertically-propagating dikes deflect to form a sill at greater depths than otherwise [Maccaferri et al., 2011]. The importance of the stress regime is greatest at the intermediate crustal levels considered here (below strength-limited very shallow levels < 3 km, and above the brittle-ductile transition). Under a compressive regime, magma chamber rupture tends to occur only where pre-existing structures are present in the overlying rock. Beneath an impact crater, the deep-going structures bounding the central uplift may act as preferential sites of chamber rupture should the magma become positively buoyant. These structures may explain why explosive volcanism occurs preferentially in impact craters on Mercury.

This begs the question of how the magma, once stalled, becomes positively buoyant, and how dikes are able to propagate to the surface despite the regional compressive stress. A major factor that enhances magma buoyancy is the presence of exsolved volatiles. As magma ascends from depth, volatiles are able to exsolve due to pressure-release. Additionally, if the magma is stored in the sub-surface, fractional crystallization of volatile-poor minerals leads to concentration of volatiles in the remaining melt and more exsolution occurs [Bower and Woods, 1997], forming a progressively-thickening low-density foam layer at the roof of the chamber [Parfitt et al., 1993]. Both deeper magma storage and a compressive tectonic regime favor buildup of exsolved volatiles because they enable a

magma chamber to remain stable up to a higher value of overpressure than it would under different conditions [Currenti and Williams, 2014].

However, because deeper storage (and thus higher pressure) inhibits the exsolution of volatiles, it may inhibit this process of exsolution, depending on the depth and volatile species involved. The evidence presented here suggests a second mode by which the volatile-content of magma can be enhanced during subsurface storage. Half of the sites sampled occur where LRM is visible at the surface. This substrate is proposed (on the basis of the apparent loss of a component of it to form hollows) to be volatile-rich [Blewett et al., 2013; Thomas et al., 2014a]. The occurrence of LRM within the walls and central uplift of many impact craters on Mercury suggests that it is present at depth at many locations where it is not apparent at the surface. It is thus possible that it is the assimilation into the magma of volatiles from wall rock of this composition during subsurface magma storage that leads to an enhanced volatile concentration in the magma chamber and therefore higher eruption velocities in explosive eruptions on Mercury than on the Moon. In this model, when LRM is encountered by magma at depth, its volatile-content lends explosivity to volcanic eruptions, while when it is exposed at the surface, the volatiles are lost less dramatically to form hollows.

This hypothesis is potentially testable: if fractional crystallization plays a major role in concentration of volatiles in explosively-erupted magmas on Mercury, pyroclastic deposits will be fractionated relative to effusive lava compositions, while if the volatile-content is derived from country rock, pyroclastic deposits need not be so fractionated. Though the resolution of compositional data currently available is not sufficient to perform this test, this is expected to be remedied by the forthcoming BepiColombo mission, set to arrive at Mercury in 2024.

4.3 Implications for the Moon and other planetary bodies

The absence of floor-fracturing in complex impact craters hosting explosive volcanism on Mercury may have implications for the causes of the association of these phenomena on the Moon. As noted in Section 4.2, unlike Mercury, the Moon is not in a state of global compression to the degree occurring on Mercury. Thus, forces favoring deeper intrusion have not been present through most or all of the

445 Moon's geological history and this alone may be sufficient for magmatic driving force to induce
446 intrusion shallow enough to cause crater floor-fracturing [Schultz, 1976]. Additionally, however,
447 many of the sampled lunar sites hosting pyroclastic volcanism, and the majority of lunar FFCs in
448 general, occur in the zone annular to mare-filled impact basins, which have a protracted history of
449 flexural extension in response to the mare load. It has been proposed that this stress state has favored
450 magma ascent from depth in these regions [Solomon and Head, 1980; McGovern et al., 2014]. We
451 suggest that it may additionally have favored shallow intrusion beneath suitably-located impact
452 craters. This would be consistent both with observations of shallow magma chambers in extensional
453 regimes on Earth [Chaussard and Amelung, 2014], and with experimental results that show
454 propagation of magma-filled cracks to higher levels than the magma's LNB where there is upwardly-
455 increasing tensile stress [Takada, 1989]. The calculated T_e of crust overlying intrusions that could
456 account for the deformation in the sampled lunar craters would allow magma storage within the
457 fallback breccia lens rather than at its base. The occurrence of floor-fractured craters, as well as
458 ancient mare pools [Schultz and Spudis, 1979], in the highlands far from mare basins indicates that
459 stresses related to mare basin loading are not the only conditions capable of enabling the rise of
460 basalts to the surface at supra-basin elevations. However, the high concentration of floor-fractured
461 craters around basin margins is consistent with the hypothesis that these stresses favor their formation.

462 FFCs also occur on Mars, and are concentrated along the boundary between the southern highlands
463 and northern plains [Schultz and Glicken, 1979; Bamberg et al., 2014], where there is evidence for a
464 history of extension [Watters and McGovern, 2006]. While some of the fractures may form by fluvial
465 processes [Sato et al., 2010], others appear to have a magmatic genesis similar to that proposed for
466 FFCs on the Moon [Schultz and Glicken, 1979; Bamberg et al., 2014]. For example, the floor-
467 fractured crater Lipany has abundant evidence for volcanic activity and none for fluvial activity and
468 lies at the margin of the Isidis basin, a region with a long history of extensional tectonics [Scott and
469 Dohm, 1990]. This indicates that some Martian FFCs and associated volcanism may be attributable to
470 flexural extension in a manner similar to those on the Moon.

5. Conclusions

A comparison of the scale of vents and surrounding deposits attributable to pyroclastic volcanism within complex impact craters on the Moon and Mercury indicates that eruptions had a significantly higher average energy on Mercury. On the Moon, this activity commonly occurs in craters with uplifted, fractured floors, but no such deformation is detected in host craters on Mercury. This evidence is most consistent with deeper magma storage prior to eruption on Mercury, in a magma chamber inhibited from upwards rupture by regional compression. Once stalled in such a reservoir, the eventual upward propagation of magma that results in a high-energy eruption is likely to have been promoted by concentration of volatiles by fractional crystallization and/or by incorporation of volatiles from wall rock.

The comparison with Mercury indicates that the absence of regional compressive stress was important in allowing shallow intrusions to form on the Moon. Further, because lunar FFCs are most common in circum-mare basin regions, which have been in flexural extension for much of their history due to the mare load, it is possible that it is not only the absence of compression but the action of extensional stresses that favored shallow intrusion in these craters. The concentration of FFCs on Mars in zones that have undergone long-term regional extension is supportive of this hypothesis, and suggests that crustal extension may play a controlling role in the formation of floor-fractured craters on terrestrial bodies in general.

Acknowledgements

Rebecca Thomas acknowledges a PhD studentship from the Science and Technology Facilities Council (UK) (ST/K502212/1). David Rothery acknowledges support from UKSA PP/E002412/1 and ST/M002101/1, and Science and Technology Facilities Council ST/L000776/1. We thank Chloé Michaut and an anonymous reviewer for their insightful and thought-provoking reviews of the original manuscript.

References

Baker, D. M. H., and J. W. Head (2013), New morphometric measurements of craters and basins on Mercury and the Moon from MESSENGER and LRO altimetry and image data: An

498 observational framework for evaluating models of peak-ring basin formation, *Planet. Space Sci.*,
499 86, 91–116, doi:10.1016/j.pss.2013.07.003.

500 Bamberg, M., R. Jaumann, H. Asche, T. Kneissl, and G. G. Michael (2014), Floor-Fractured Craters
501 on Mars – Observations and Origin, *Planet. Space Sci.*, 98, 146–162,
502 doi:10.1016/j.pss.2013.09.017.

503 Barnouin, O. S., C. E. Ernst, J. T. Heinick, S. Sugita, M. J. Cintala, D. A. Crawford, and T. Matsui
504 (2011), Experimental results investigating the impact velocity effects on crater growth and the
505 transient crater diameter-to-depth ratio, *Lunar Planet. Inst. Sci. Conf. Abstr.*, 42, 2258.

506 Barnouin, O. S., M. T. Zuber, D. E. Smith, G. A. Neumann, R. R. Herrick, J. E. Chappelow, S. L.
507 Murchie, and L. M. Prockter (2012), The morphology of craters on Mercury: Results from
508 MESSENGER flybys, *Icarus*, 219(1), 414–427, doi:10.1016/j.icarus.2012.02.029.

509 Blewett, D. T. et al. (2013), Mercury’s hollows: Constraints on formation and composition from
510 analysis of geological setting and spectral reflectance, *J. Geophys. Res. - Planets*, 118(5), 1013–
511 1032.

512 Bower, S. M., and A. W. Woods (1997), Control of magma volatile content and chamber depth on the
513 mass erupted during explosive volcanic eruptions, *J. Geophys. Res.*, 102(B5), 10273–10290.

514 Byrne, P. K., C. Klimczak, A. M. C. Şengör, S. C. Solomon, T. R. Watters, and S. A. Hauck (2014),
515 Mercury’s global contraction much greater than earlier estimates, *Nat. Geosci.*, 7(April), 301–
516 307, doi:10.1038/NGEO2097.

517 Chaussard, E., and F. Amelung (2014), Regional controls on magma ascent and storage in volcanic
518 arcs, *Geochemistry, Geophys. Geosystems*, 15(4), 1407–1418, doi:10.1002/2013GC005216.

519 Cintala, M. J. (1979), Mercurian crater rim heights and some interplanetary comparisons, *Lunar*
520 *Planet. Sci. Conf. Proc.*, 10.

521 Collins, G. S. (2014), Numerical simulations of impact crater formation with dilatancy, *J. Geophys.*
522 *Res. Planets*, doi:10.1002/2014JE004708.

523 Coombs, C. R., and B. R. Hawke (1992), Pyroclastic deposits on the western limb of the Moon, *Proc.*
524 *Lunar Planet. Sci.*, 22, 303–312.

525 Croft, S. K. (1985), The scaling of complex craters, *J. Geophys. Res. Solid Earth*, 90(S02), C828–
526 C842.

527 Currenti, G., and C. A. Williams (2014), Numerical modeling of deformation and stress fields around
528 a magma chamber: Constraints on failure conditions and rheology, *Phys. Earth Planet. Inter.*,
529 226, 14–27, doi:10.1016/j.pepi.2013.11.003.

530 Denevi, B. W. et al. (2013), The distribution and origin of smooth plains on Mercury, *J. Geophys.*
531 *Res. Planets*, 118(5), 891–907, doi:10.1002/jgre.20075.

532 Gaddis, L. R., M. I. Staid, J. a Tyburczy, B. R. Hawke, and N. E. Petro (2003), Compositional
533 analyses of lunar pyroclastic deposits, *Icarus*, 161(2), 262–280, doi:10.1016/S0019-
534 1035(02)00036-2.

535 Gillis-Davis, J. J., D. T. Blewett, R. W. Gaskell, B. W. Denevi, M. S. Robinson, R. G. Strom, S. C.
536 Solomon, and A. L. Sprague (2009), Pit-floor craters on Mercury: Evidence of near-surface
537 igneous activity, *Earth Planet. Sci. Lett.*, 285(3-4), 243–250, doi:10.1016/j.epsl.2009.05.023.

538 Grieve, R. A. F., and M. J. Cintala (1982), A method for estimating the initial impact conditions of
539 terrestrial cratering events, exemplified by its application to Brent crater, Ontario, *Lunar Planet.*
540 *Sci. Conf. Proc.*, 12, 1607–1621.

541 Grieve, R. A. F., and M. J. Cintala (1997), Planetary differences in impact melting, *Adv. Sp. Res.*,
542 20(8), 1551–1560, doi:10.1016/S0273-1177(97)00877-6.

543 Gustafson, J. O., J. F. Bell, L. R. Gaddis, B. R. Hawke, and T. A. Giguere (2012), Characterization of
544 previously unidentified lunar pyroclastic deposits using Lunar Reconnaissance Orbiter Camera
545 data, *J. Geophys. Res. Planets*, 117(E12), doi:10.1029/2011JE003893.

546 Hall, J. L., S. C. Solomon, and J. W. Head (1981), Lunar floor-fractured craters: Evidence for viscous
547 relaxation of crater topography, *J. Geophys. Res.*, 86(B10), 9537–9552.

548 Head, J. W., and L. Wilson (1979), Alphonsus-type dark-halo craters: Morphology, morphometry and
549 eruption conditions, *Lunar Planet. Sci. Conf. Proc.*, 10, 2861–2897.

550 Head, J. W., and L. Wilson (1992), Lunar mare volcanism: Stratigraphy, eruption conditions, and the
551 evolution of secondary crusts, *Geochim. Cosmochim. Acta*, 56, 2155–2175.

552 Head, J. W. et al. (2009), Evidence for intrusive activity on Mercury from the first MESSENGER
553 flyby, *Earth Planet. Sci. Lett.*, 285(3-4), 251–262, doi:10.1016/j.epsl.2009.03.007.

554 Jozwiak, L. M., J. W. Head, M. T. Zuber, D. E. Smith, and G. A. Neumann (2012), Lunar floor-
555 fractured craters: Classification, distribution, origin and implications for magmatism and shallow
556 crustal structure, *J. Geophys. Res.*, 117(E11), E11005, doi:10.1029/2012JE004134.

557 Jozwiak, L. M., J. W. Head, and L. Wilson (2015), Lunar floor-fractured craters as magmatic
558 intrusions: Geometry, modes of emplacement, associated tectonic and volcanic features, and
559 implications for gravity anomalies, *Icarus*, 248, 424–447, doi:10.1016/j.icarus.2014.10.052.

560 Vander Kaaden, K. E., C. B. Agee, and F. M. McCubbin (2015), Density and compressibility of the
561 molten lunar picritic glasses: Implications for the roles of Ti and Fe in the structures of silicate
562 melts, *Geochim. Cosmochim. Acta*, 149, 1–20, doi:10.1016/j.gca.2014.10.029.

563 Kenkmann, T., M. H. Poelchau, and G. Wulf (2014), Structural geology of impact craters, *J. Struct.*
564 *Geol.*, 62, 156–182, doi:10.1016/j.jsg.2014.01.015.

565 Kerber, L., J. W. Head, S. C. Solomon, S. L. Murchie, D. T. Blewett, and L. Wilson (2009), Explosive
566 volcanic eruptions on Mercury: Eruption conditions, magma volatile content, and implications
567 for interior volatile abundances, *Earth Planet. Sci. Lett.*, 285(3-4), 263–271,
568 doi:10.1016/j.epsl.2009.04.037.

569 Kerber, L., J. W. Head, D. T. Blewett, S. C. Solomon, L. Wilson, S. L. Murchie, M. S. Robinson, B.
570 W. Denevi, and D. L. Domingue (2011), The global distribution of pyroclastic deposits on
571 Mercury: The view from MESSENGER flybys 1–3, *Planet. Space Sci.*, 59(15), 1895–1909,
572 doi:10.1016/j.pss.2011.03.020.

573 Maccaferri, F., M. Bonafede, and E. Rivalta (2011), A quantitative study of the mechanisms
574 governing dike propagation, dike arrest and sill formation, *J. Volcanol. Geotherm. Res.*, 208(1-
575 2), 39–50, doi:10.1016/j.jvolgeores.2011.09.001.

576 McGovern, P. J., W. S. Kiefer, Y. Kramer, M. T. Zuber, J. C. Andrews-Hanna, and J. W. H. III
577 (2014), Magma ascent at lunar impact basins: effects of lithospheric tectonic stress gradients,
578 brittle failure, and volatile generation, *Lunar Planet. Sci. Conf.*, 45, 2771.

579 Menand, T. (2011), Physical controls and depth of emplacement of igneous bodies: A review,
580 *Tectonophysics*, 500(1-4), 11–19, doi:10.1016/j.tecto.2009.10.016.

581 Moratto, S. Z. M., M. J. Broxton, R. A. Beyer, M. Lundy, and K. Husmann (2010), Ames Stereo
582 Pipeline, NASA's open source automated stereogrammetry, *Lunar Planet. Sci. Conf.*, 41, 2364.

583 Murchie, S. L. et al. (2015), Orbital multispectral mapping of Mercury with the MESSENGER
584 Mercury Dual Imaging System: Evidence for the origins of plains units and low-reflectance
585 material, *Icarus*, 254, 287–305, doi:10.1016/j.icarus.2015.03.027.

586 Parfitt, E. A., L. Wilson, and J. W. Head (1993), Basaltic magma reservoirs: Factors controlling their
587 rupture characteristics and evolution, *J. Volcanol. Geotherm. Res.*, 55(1-2), 1–14,
588 doi:10.1016/0377-0273(93)90086-7.

589 Pike, R. J. (1980), Geometric interpretation of lunar craters, *US Geol. Soc. Prof. Pap. 1046 -C*, C1–
590 C77.

591 Pike, R. J. (1988), Geomorphology of impact craters on Mercury, in *Mercury*, edited by F. Vilas, C.
592 R. Chapman, and M. S. Matthews, pp. 165–273, University of Arizona Press, Tucson, AZ.

593 Pollard, D. D., and A. M. Johnson (1973), Mechanics of growth of some laccolithic intrusions in the
594 Henry Mountains, Utah, II. Bending and failure of overburden layers and sill formation,
595 *Tectonophysics*, 18, 311–354.

596 Rothery, D. A., R. J. Thomas, and L. Kerber (2014), Prolonged eruptive history of a compound
597 volcano on Mercury: volcanic and tectonic implications, *Earth Planet. Sci. Lett.*, 385, 59–67.

598 Sato, H., K. Kurita, and D. Baratoux (2010), The formation of floor-fractured craters in Xanthe Terra,
599 *Icarus*, 207(1), 248–264, doi:10.1016/j.icarus.2009.10.023.

600 Scholz, C. A., T. Karp, K. M. Brooks, P. Y. O. Milkereit, Bernd, Amoako, and J. A. Arko (2002),
601 Pronounced central uplift identified in the Bosumtwi impact structure, Ghana, using
602 multichannel seismic reflection data, *Geology*, 30(10), 939–942.

603 Schultz, P. H. (1976), Floor-fractured lunar craters, *Moon*, 15, 241–273, doi:10.1007/BF00562240.

604 Schultz, P. H., and H. Glicken (1979), Impact crater and basin control of igneous processes on Mars,
605 *J. Geophys. Res.*, 84(9), 8033–8047.

606 Schultz, P. H., and P. D. Spudis (1979), Evidence for ancient mare volcanism, *Proc. Lunar Planet.*
607 *Sci. Conf.*, 10, 2899–2918.

608 Scott, D. H., and J. M. Dohm (1990), Chronology and global distribution of fault and ridge systems
609 on Mars, *Proc. 20th Lunar Planet. Sci. Conf.*, 487–501.

610 Senft, L. E., and S. T. Stewart (2009), Dynamic fault weakening and the formation of large impact
611 craters, *Earth Planet. Sci. Lett.*, 287(3-4), 471–482, doi:10.1016/j.epsl.2009.08.033.

612 Solomon, S. C., and J. W. Head (1980), Lunar Mascon Basins: Lava Filling, Tectonics, and Evolution
613 of the Lithosphere, *Rev. Geophys. Sp. Phys.*, 18(1), 107–141.

614 Strom, R. G., N. J. Trask, and J. E. Guest (1975), Tectonism and volcanism on Mercury, *J. Geophys.*
615 *Res.*, 80(17), 2478–2507, doi:10.1029/JB080i017p02478.

616 Takada, A. (1989), Magma transport and reservoir formation by a system of propagating cracks, *Bull.*
617 *Volcanol.*, 52(2), 118–126.

618 Thomas, R. J., D. A. Rothery, S. J. Conway, and M. Anand (2014a), Hollows on Mercury: Materials
619 and mechanisms involved in their formation, *Icarus*, 229, 221–235,
620 doi:10.1016/j.icarus.2013.11.018.

621 Thomas, R. J., D. A. Rothery, S. J. Conway, and M. Anand (2014b), Mechanisms of explosive
622 volcanism on Mercury: implications from its global distribution and morphology, *J. Geophys.*
623 *Res. Planets*, 119, 2239–2254, doi:10.1002/2014JE004692.

624 Thomas, R. J., A. Lucchetti, G. Cremonese, D. A. Rothery, M. Massironi, C. Re, S. J. Conway, and
625 M. Anand (2015), A cone on Mercury: Analysis of a residual central peak encircled by an
626 explosive volcanic vent, *Planet. Space Sci.*, 108, 108–116, doi:10.1016/j.pss.2015.01.005.

627 Thorey, C., and C. Michaut (2014), A model for the dynamics of crater-centered intrusion:
628 Application to lunar floor-fractured craters, *J. Geophys. Res. Planets*, 119, 286–312,
629 doi:10.1002/2013JE004467.

630 Watters, T. R., and P. J. McGovern (2006), Lithospheric flexure and the evolution of the dichotomy
631 boundary on Mars, *Geophys. Res. Lett.*, 33(8), doi:10.1029/2005GL024325.

632 Watters, T. R. et al. (2010), Evidence of recent thrust faulting on the Moon revealed by the Lunar
633 Reconnaissance Orbiter Camera, *Science*, 329(5994), 936–940.

634 Weider, S. Z. et al. (2015), Evidence for geochemical terranes on Mercury: Global mapping of major
635 elements with MESSENGER's X-Ray Spectrometer, *Earth Planet. Sci. Lett.*, 416, 109–120,
636 doi:10.1016/j.epsl.2015.01.023.

637 Wichman, R. W., and P. H. Schultz (1995a), Floor-fractured craters in Mare Smythii and west of
638 Oceanus Procellarum: Implications of crater modification by viscous relaxation and igneous
639 intrusion models, *J. Geophys. Res.*, 100(E10), 21201–21218.

640 Wichman, R. W., and P. H. Schultz (1995b), Floor-fractured impact craters on Venus: Implications
641 for igneous crater modification and local magmatism, *J. Geophys. Res.*, 100(E2), 3233–3244.

642 Wieczorek, M. A., M. T. Zuber, and R. J. Phillips (2001), The role of magma buoyancy on the
643 eruption of lunar basalts, *Earth Planet. Sci. Lett.*, 185(1), 71–83, doi:10.1016/S0012-
644 821X(00)00355-1.

645 Wieczorek, M. A. et al. (2013), The crust of the Moon as seen by GRAIL, *Science*, 339(6120), 671–
646 675, doi:10.1126/science.1231530.

- 647 Wilson, L. (1980), Relationships between pressure, volatile content and ejecta velocity in three types
648 of volcanic explosion, *J. Volcanol. Geotherm. Res.*, 8, 297–313.
- 649 Wilson, L., and E. A. Parfitt (1989), The influence of gravity on planetary volcanic eruption rates: A
650 reappraisal, *Lunar Planet. Sci. Conf. Abstr.*, 20, 1213.
- 651 Wolfe, R. W., and F. El-Baz (1976), Photogeology of the multi-ringed crater Haldane in Mare
652 Smythii, *Lunar Planet. Sci. Conf. Proc.*, 7, 2903–2912.
- 653